Indian Journal of Chemistry
Vol. 63, May 2024, pp. 485-494
DOI: 10.56042/ijc.v63i5.9153

# Investigating the effect of doping $LaCoO_3$ in $CoFe_2O_4$ forming nanocomposite, towards oxygen evolution and methanol oxidation reactions in alkaline medium

Reena Parihar, Prakhar Mishra, Yamini Singh & Narendra Kumar Singh*

Department of Chemistry, Faculty of Science, University of Lucknow, Lucknow 226 007, India

E-mail: nksbhu@yahoo.com, singh_narendra@lkouniv.ac.in

*Received 28 February 2024; accepted (revised) 24 April 2024*

$CoFe_2O_4$-$LaCoO_3$ was synthesized employing a two-step, low-temperature wet chemical method involving co-precipitation and sol-gel techniques. The co-precipitation process was employed to prepare $CoFe_2O_4$, with *p*H regulation at 11 using NaOH solution. Subsequently, $CoFe_2O_4$-$LaCoO_3$ was synthesized *via* sol-gel process. The synthesized materials were subjected to physicochemical analysis using Fourier Transform Infrared spectroscopy (FTIR), X-ray diffraction (XRD) and Scanning Electron Microscopy (SEM). The electrocatalytic properties of these materials were evaluated in terms of their performance towards oxygen evolution reaction (OER) and methanol oxidation reaction (MOR) in alkaline medium. The redox behaviour of the materials was characterized through cyclic voltammetry analysis in 1M KOH solution. The electrocatalytic activity of the materials, when assessed using anodic polarization curves revealed that $CoFe_2O_4$-$LaCoO_3$ exhibited higher activity, with current densities of 1.6 mA $cm^{-2}$ for OER and 9.2 mA $cm^{-2}$ for MOR recorded at 650 mV. Further, the thermodynamic parameters like standard enthalpy of activation ($\Delta H^{\circ\#}$), standard entropy of activation ($\Delta S^{\circ\#}$) and standard electrochemical energy of activation ($\Delta H_{el}^{\circ\#}$) were calculated by recording anodic polarization curve in KOH as well as KOH with $CH_3OH$ solutions at various temperatures. The findings presented in this study demonstrate the promising electrocatalytic performance of $CoFe_2O_4$-$LaCoO_3$ film electrode for applications in OER and MOR under alkaline condition.

**Keywords**: Nanocomposite, Sol-gel procedure, XRD, Oxygen evolution reaction, Methanol oxidation reaction

Since excessive fossil fuel consumption pollutes the environment, clean, renewable energy sources and highly effective, low-cost energy storage systems are urgently required[1,2]. The typical electrochemical systems for energy storage and conversion innovations are water splitting, fuel cells, Li- ion batteries (LIBs) and supercapacitors[3]. Various materials such as noble-metals, carbon-based materials such as carbon nanotube, N-doped carbon, graphitic carbon nitride, graphene, graphene oxide, *etc.*, oxides, oxy-hydroxides and alloys of Ni, Mn, Fe and Co, *etc.* and their composite with carbon as well as spinel and perovskite structures have been examined as electrocatalysts for OER[4-16]. Owing to their higher energy conversion efficiency, high stability and simple set-up, direct methanol fuel cells (DMFC) are regarded a promising contender for power production[17-19]. Various electrocatalysts (anode materials) such as Pt[20-24], Pt-Ru alloys[20,25-28], $WO_x$[29], graphite[30], multiwalled carbon nanotubes (MWCNTs)[31], nanowire array[32], oxides of V, Fe, Ni, In, Sn, La and Pb[33], non-noble metallic glasses[34] and carbides[35] were developed and studied for their electrocatalytic activity towards MOR.

Because of their wide range of practical applications, nanocomposites of transition metal oxides have received much interest as a potential candidate in nearly all branches of science[36]. Several nanocomposites of transition metal oxides for their practical applications have been described in literature including CuO–ZnO as an antibacterial agent[37], Polyaniline/ZnO as sensor[38], CNT–ZnO as an electrode material for supercapacitor[39], Graphene–ZnO as photovoltaic cells[40] and GO/ZnO in photocatalytic degradation of basic fuchsin dye[41]. Several methods have been employed for the synthesis of nanocomposites of transition metal oxides such as co-precipitation method[42], sol-gel technique[43], hydrothermal technique[44], chemical vapor deposition[45], wet chemical method[46], microwave assisted method[47] and green method[48]. These methods produce material with enhanced surface area, enhanced porosity and homogeneity[36].

$BiFeO_3$-$NiFe_2O_4$/$ZnFe_2O_4$/$CoFe_2O_4$ composites of varying composition were synthesized *via* sol-gel technique and investigated towards the structural, electrical and magnetic properties[49]. Likewise, $CoFe_2O_4$–$BiFeO_3$[50], $LaFeO_3$-$NiFe_2O_4$[51] and $BiFeO_3$–

$NiFe_2O_4$ nanocomposites[52] were examined towards their structural, electrical and magnetic properties. Composites of spinel oxide-perovskite oxide have been little explored for their catalytic performance with regard to OER and MOR.

Therefore, we aim to expand our research and synthesize composite of spinel oxide [$CoFe_2O_4$ (defined as CFO hereafter)] and perovskite oxide [$LaCoO_3$ (defined as LCO hereafter)]; forming $CoFe_2O_4$-$LaCoO_3$ defined as CFO-LCO hereafter] using low temperature sol gel technique and studied their catalytic performance with regards to OER and MOR in alkaline medium. In this paper, the findings of the study are discussed.

## Experimental Section

### Synthesis of CFO

Spinel oxide, specifically CFO, was synthesized *via* the co-precipitation technique with precision. A stoichiometric quantity of $Co(NO_3)_2 \cdot 6H_2O$ (MERCK, 97%) and $Fe(NO_3)_3 \cdot 9H_2O$ (MERCK, 98%) was dissolved in double-distilled water. The *p*H was meticulously maintained at 11 by the gradual addition of 5M NaOH solution. Subsequently, the solution underwent continuous stirring for 1 hour at 65°C on a hot plate magnetic stirrer. Following this, it was filtered and subjected thorough washing with double-distilled water. Finally, the resulting precipitates were dried overnight at 190°C, ground into a fine powder, and then grieved heat treatment at 650°C for 1 hour[53].

### Synthesis of nanocomposite

The preparation of composite was done by simple sol-gel technique. In the typical process, the stoichiometric quantity of $La(NO_3)_3.6H_2O$ (HIMEDIA, 99%) and $Co(NO_3)_2.6H_2O$ (MERCK, 97%) were dissolved in double distilled water and 4 ml of ethylene glycol was added to it. A suitable amount of synthesized CFO was added and the solution stirred continuously for 3h at 80°C. Thereafter, the sol was heated in a water bath till a gel-like mass achieved, this gel was reheated above 150°C on a hot plate until precursor of CFO-LCO was obtained. Finally, nanocomposite of CFO-LCO was obtained by sintering the precursor at 650°C for 1h[53].

The physicochemical characterization of synthesized materials has been done by FTIR in the wavenumber range of 4000-400 $cm^{-1}$ by using Shimadzu (IRAFFINITY-1S CE) spectrometer. The XRD pattern recorded with a Bruker D8 Advance X-ray diffractometer fitted with a radiation source; Cu-Kα, λ=1.54 Å was used to determine the phase and crystallite size of the materials. The electrocatalysts were also analysed for their morphological studies by SEM images using JEOL scanning electron microscopy (JSM 7600 F). The electrochemical studies were carried out by coating the electrocatalysts over the pre-treated Ni-substrate using oxide slurry painting procedure as reported in literature[54], transforming them into electrode. Electrochemical tests were done using Gamry Reference 600 ZRA fitted with a potentiostat/galvanostat. The film electrode was taken as the working electrode, pre-treated Pt-Foil as the counter electrode and Hg/HgO/1M KOH as the reference electrode.

## Results and Discussion

### Physicochemical Analysis

### FTIR Spectroscopy

The formation of spinel oxide and the novel composite has been confirmed by FTIR spectra as shown in Fig. 1(A). The band at 586 $cm^{-1}$ in the

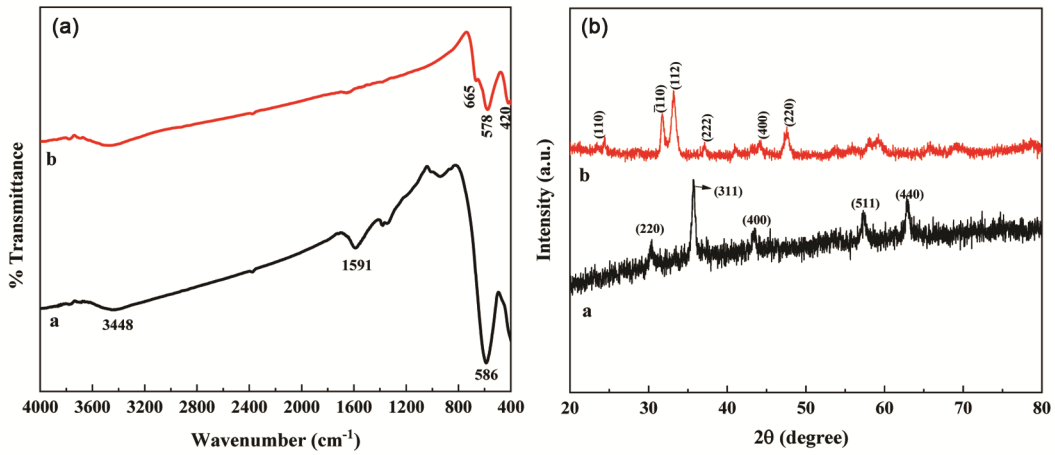


Fig. 1 — (A): FTIR Spectra of (a): CFO, (b): CFO-LCO, (B): XRD powder patterns of (a): CFO, (b): CFO-LCO sintered at 650°C for 1h

Table 1 — XRD data of CFO & CFO-LCO

| Oxides | Phase | 2θ (deg) | hkl | Crystallite Size (nm) | ICDD No. |
|---|---|---|---|---|---|
| CFO | – | 30.064 | 220 | 19.2 | 00-003-0864 |
| | | 35.452 | 311 | | |
| | | 43.473 | 400 | | |
| | | 57.168 | 511 | | |
| | | 62.728 | 440 | | |
| CFO-LCO | CFO | 37.279 | 222 | 17.4 | 00-001-112-01-084-0847 |
| | | 43.479 | 400 | | |
| | LCO | 23.333 | 110 | | |
| | | 32.984 | $\bar{1}10$ | | |
| | | 33.484 | 112 | | |
| | | 47.716 | 220 | | |

spectra of CFO owing to the existence of ferrite oxide[55] due to asymmetric stretching mode of M-O bond in tetrahedral and octahedral positions where $Co^{2+}$ ions reside in the octahedral-site while $Fe^{3+}$ ions reside in both octahedral and tetrahedral sites[56]. Also, there seems few small disturbances between 420-665 $cm^{-1}$ suggesting the presence of spinel and perovskite oxide in composite[57]. The broad peak at 3448 $cm^{-1}$ & 1591 $cm^{-1}$ corresponds to the stretching and bending vibration modes due to water molecules[58].

## X-ray diffraction (XRD)

Fig. 1(B) displays the XRD spectra of synthesized materials at 650 ℃ that were recorded in 20° to 80° 2 theta values. The XRD patterns indicated clearly the formation of composite material with two phases (spinel and perovskite phase). The obtained patterns match very close to their respective ICDD Card No. given in Table 1. With the help of Scherer's formula[59], the crystallite size as shown in Table 1, of synthesized materials has been calculated and found to be 17 and 19 nm for CFO-LCO and CFO, respectively.

$$D = \frac{0.9\,\lambda}{\beta \mathrm{Cos}\theta} \quad \ldots (1)$$

where, λ is the wavelength of Cu-$K_\alpha$ radiation source, β is the full width at half maximum of peak (FWHM) and θ is the diffraction angle.

## Scanning Electron Microscopy (SEM)

The morphology of the synthesized spinel oxide & composite sintered at 650°C for 1h at the magnification x100,000 was examined through scanning electron microscopy, as depicted in Fig. 2. Composite material [Fig. 2(b)] shows three-dimensionalflower like morphology with

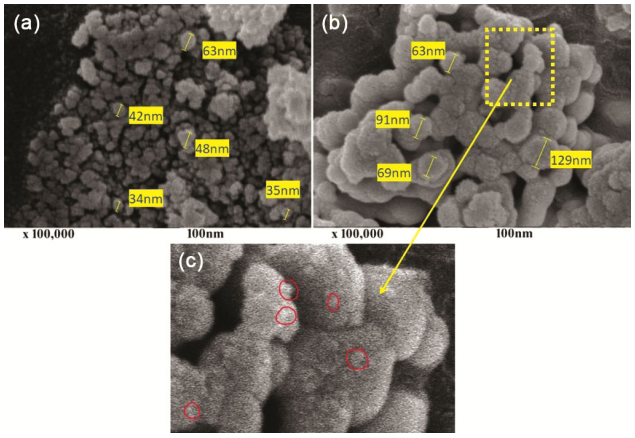


Fig. 2 — SEM images of (a): CFO, (b): CFO-LCO sintered at 650° C for 1h, (c) embedded doped particles over core shell of CFO

agglomeration of both CFO and LCO and having bigger size (63-129 nm) as compared to CFO (34-63 nm). Small particles of CFO are seen to be compact in the composite material [Fig. 2(c)]. This might be due to the formation of gel during synthesis in which sodium hydroxide is wreathed to form a complex network structure in the space. The powder that is obtained when the gel is dried, enables the creation of a three-dimensional network structure. Fig. 2(a) depicts that the obtained powder is made up of distributed smaller primary particles of spinel oxide (CFO). Average particle size of the materials has been estimated and found to be 44.4 nm for CFO & 97.2 nm for CFO-LCO.

## Electrochemical Analysis

## Oxygen Evolution Reaction (OER)

## Cyclic Voltammetry (CV)

The electrocatalysts were examined with regard to OER by recording cyclic voltammetry in 1M KOH.

Fig. 3(A) represents the cyclic voltammogram of electrocatalysts over Ni-substrate in the potential region of 0.0 to 0.7V in 1M KOH. A couple of redox peaks was observed in case of each electrocatalyst prior to OER. The position of redox peaks is found to be similar with redox couple of Ni(III)/Ni(II)[54,60]. The observed redox peaks correspond to the oxidation and reduction reaction taking place at Ni-substrate due to electrical contact with electrolyte *via* cracks, pores and grain boundaries. Also, the oxides synthesised from these methodologies shows hydrophilic behaviour and they hydrate in aqueous solution, wetting the entire film thickness[61]. Based on the CV curve, the estimated values of the anodic peak potential ($E_{Pa}$), cathodic peak potential ($E_{Pc}$), peak separation potential ($\Delta E_p = E_{Pa} - E_{Pc}$), formal redox potential ($E^o = (E_{Pa}+E_{Pc})/2$), anodic peak current density ($j_{Pa}$), cathodic peak current density ($j_{Pc}$) and voltametric charge (q) are shown in Table 2. The onset potential for OER has been compared for the electrocatalysts CFO & CFO-LCO and was found to be 0.59 V and 0.57 V, respectively. This clearly shows that the oxygen evolution starts at comparatively low potential with CFO-LCO film electrode.

The influence of scan rate on the redox process was also studied and found to be comparable as stated in literature[62]. Fig. 3(B) displays the cyclic voltammogram for the Ni/CFO-LCO at varying scan rates. The characteristics of the cyclic voltammogram acquired at various scan rates are comparable to that seen at scan rate of 20 $mVsec^{-1}$. However, the anodic and cathodic peaks were relocated to the top and bottom potential sides, respectively with an increase

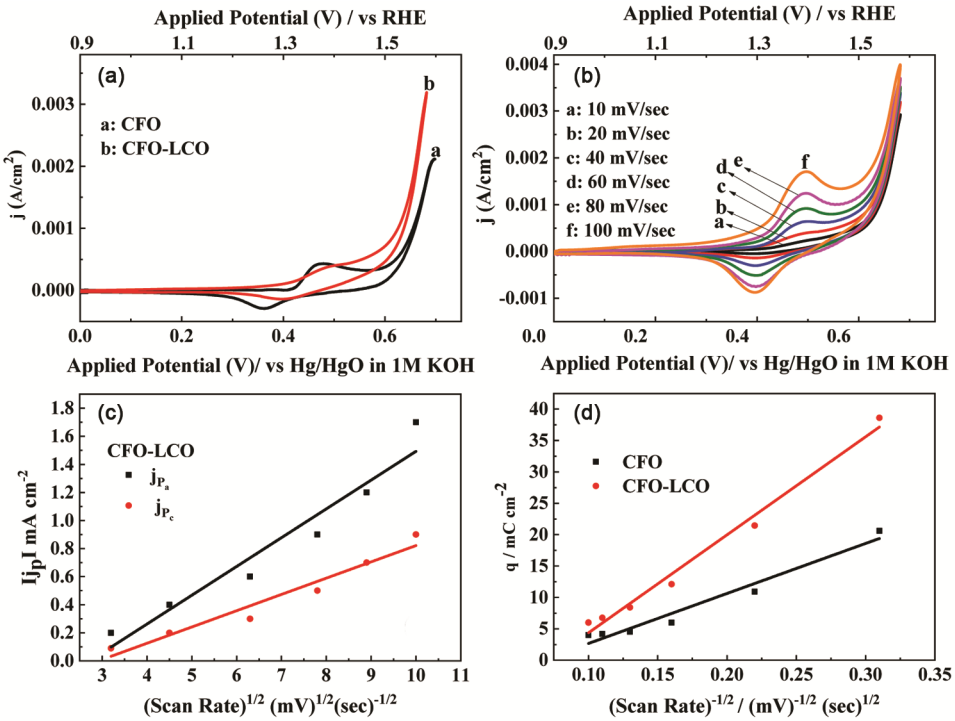


Fig. 3 — (A): CV Curve of Ni/CFO & CFO-LCO(scan rate = 20 mV/sec), (B): Cyclic voltammogram of Ni/CFO-LCO film electrode at different scan rates, (C): Plot of $|j_P|$ *vs* (scan rate)$^{1/2}$ for Ni/CFO-LCO film electrode, (D): Plot of voltammetric charge (q) *vs* (scan rate)$^{-1/2}$ for Ni/CFO & CFO-LCO in 1M KOH at 25℃

Table 2 — Values of the cyclic voltammetric parameters for CFO & CFO-LCO in

| Electrode | $E_{Pa}$ /mV | $E_{Pc}$ /mV | $\Delta E_p$ /mV | $E^o = (E_{Pa}+E_{Pc})/2$ / mV | $\lvert j_{Pa}\rvert$/ mA $cm^{-2}$ | $\lvert j_{Pc}\rvert$/ mA $cm^{-2}$ | $\lvert j_{Pa}\rvert/\lvert j_{Pc}\rvert$ | q/ mC $cm^{-2}$ |
|---|---|---|---|---|---|---|---|---|
| CFO | 479 | 361 | 118 | 420 | 0.4 | 0.3 | 1.3 | 10.9 |
| CFO-LCO | 483 | 396 | 87 | 440 | 0.3 | 0.2 | 1.5 | 21.5 |

1M KOH at 25°C (scan rate = 20 $mVsec^{-1}$)

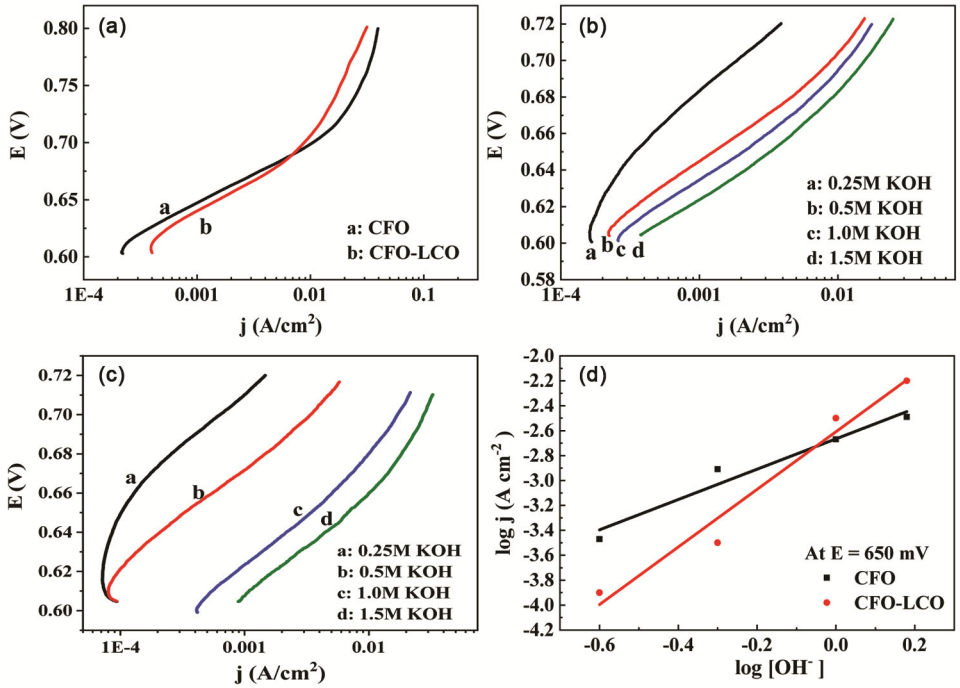


Fig. 4 — (A): Tafel plots for $O_2$ evolution on Ni/CFO & CFO-LCO in 1M KOH at 25℃; scan rate: 0.2 $mVsec^{-1}$,(B): Tafel plots for $O_2$ evolution on Ni/CFO at varying KOH concentrations at 25℃, (C): Tafel plots for $O_2$ evolution on Ni/CFO-LCO at varying KOH concentrations at 25℃, (D): Plot of log j *vs* log [$OH^-$] for Ni/CFO & CFO-LCOelectrodes at 650 mV

Table 3 — Electrode kinetic parameters for OER on CFO & CFO-LCO electrodes in 1M KOH at 25°C

| Electrode | Loading (mg $cm^{-2}$) | Order (p) | Tafel Slope (b) | Apparent Current density ($mA/cm^2$) at E = 650 mV | Specific activity ($mAcm^{-2}/g$)×$10^{-3}$ at E = 650 mV |
|---|---|---|---|---|---|
| CFO | 9.5 | 1.2 | 52 | 1.1 | 0.1 |
| CFO-LCO | 9.9 | 2.3 | 54 | 1.6 | 0.2 |

in scan rate from 10 to 100 $mVsec^{-1}$ indicating effective catalysis because improved charge transfer phenomena under alkaline conditions lead to superior capabilities[63]. The anodic and cathodic peaks on either side were observed to shift with increasing scan rate implying that the oxidation/reduction process is quasi reversible[64-68].Furthermore, fraction of anodic to cathodic peak current found to be greater than 1, signifying the irreversibility of the oxidation/reduction process[69,70].

For CFO-LCO, $j_{Pa}$ and $j_{Pc}$ were constructed against (scan rate)$^{1/2}$ as shown in Fig. 3(C). The voltammetric charge (q) was also constructed against (scan rate)$^{-1/2}$ for electrocatalysts as displayed in Fig. 3(D). The voltammetric charge was calculated by integrating the CV curve from potential zero up to the potential just prior to the OER. The straight line obtained in both the figures indicates that the surface redox behaviour is diffusion controlled[61].

## Electrocatalytic Activity

The catalytic performance of prepared electrocatalysts was examined *via* anodic polarization curve recorded at a steady scan rate of 0.2 $mVsec^{-1}$ in 1M KOH as shown in Fig. 4(A). The electrode kinetic parameters for OER were estimated using the Tafel plot and values are tabulated in Table 3. When catalytic performance was compared in terms of current density at E = 650 mV, CFO-LCO (j = 1.6 $mAcm^{-2}$) film electrode was found to be more active towards OER. This is due to change in morphology as supported by the SEM images.

The order of OER with electrocatalysts was calculated from the Tafel plots recorded in different concentration of KOH solution (0.25M–1.5M KOH) at 25°C. The electrolytic solution's ionic strength was retained at 1.5 by employing $KNO_3$. A characteristic curve for Ni/CFOand Ni/CFO-LCO is presented in Fig. 4(B) and (C). A log j *vs* log [$OH^-$] plot was

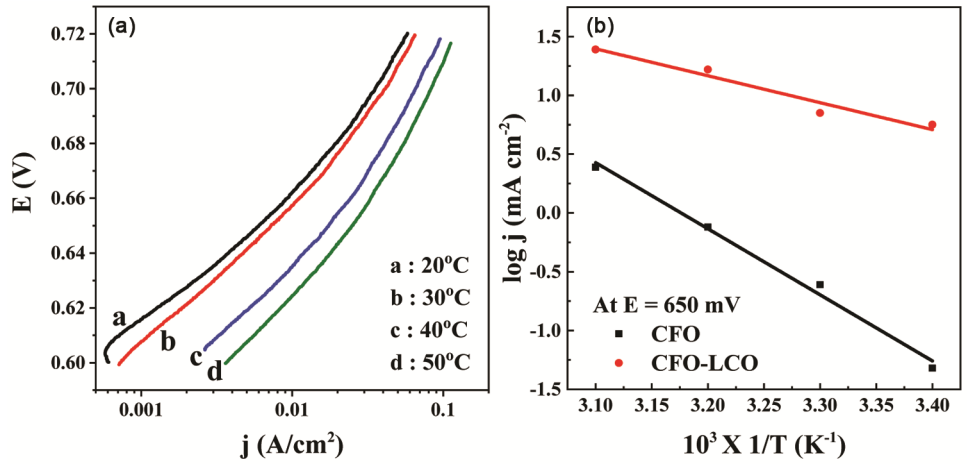


Fig. 5 — (A): Anodic Polarization Curve for Ni/CFO-LCO film electrode at different temperatures, (B): The Arrhenius plot for Ni/CFO & CFO-LCO at E = 650 mV in 1M KOH

Table 4 — Thermodynamic parameters for $O_2$ evolution on Ni/CFO & CFO-LCO in 1M KOH

| Electrode | $\Delta H_{el}^{\circ\#}$ (kJmol$^{-1}$) at E = 700mV | $\Delta S^{\circ\#}$ (Jdeg$^{-1}$mol$^{-1}$) | $\Delta H^{\circ\#}$ (kJmol$^{-1}$) |
|---|---|---|---|
| CFO | 89.8 | 48.4 | 122.8 |
| CFO-LCO | 25.5 | 230.0 | 68.2 |

constructed for electrocatalysts at E = 650 mV as shown in Fig. 4(D). The order of reaction was calculated by the gradient of straight line and values are tabulated in Table 3.

The activity of the electrocatalysts is represented in the form of specific activity (current density per gram) and is estimated by the following relation:

$$\text{Specific Activity} = \frac{Apparent\ Current\ Density}{Mterial\ Loading\ (mg\ cm^{-2})} \quad \ldots (2)$$

**Thermodynamic Parameters**

The thermodynamic study of OER has been meticulously determined by the Tafel experiments conducted over a temperature window ranging from 20°C-50°C of 1M KOH. Figure 5 (A) depicts a characteristic curve obtained for CFO-LCO. The value of $\Delta H_{el}^{\circ\#}$ was determined from the gradient of log j vs 1/T plot [Figure 5 (B)].

$\Delta H^{\circ\#}$ and $\Delta S^{\circ\#}$ were estimated from the relations (3) and (4)[71,72], respectively:

$$\Delta H_{el}^{\circ\#} = \Delta H^{\circ\#} - \alpha F\eta \quad \ldots (3)$$

In above equation, α is the transfer coefficient given by 2.303RT/bF, here R, T and F are the gas constant, absolute temperature and Faraday constant, respectively. 'b' denotes the Tafel slope evaluated from the Tafel plots acquired at various temperatures and η is the overpotential determined by the relation $\eta = E - E_{O_2/OH^-}$, where E is the applied potential and $E_{O_2/OH^-}$ (= 0.303 V vs. Hg/HgO)[73] is the theoretical equilibrium Nernst potential in 1M KOH at 25°C.

$$\Delta S^{\circ\#} = 2.3R\ [\log j + \Delta H_{el}^{\circ\#}\ /2.3RT - \log (nF\omega C_{OH^-})] \quad \ldots (4)$$

In above equation, ω is the frequency term given by $k_BT/h$, here, $k_B$ is the Boltzmann constant and h is the Plank's constant.

Thermodynamic parameters were calculated for electrocatalysts and are given in Table 4. The value of $\Delta H_{el}^{\circ\#}$ was found to be 89.8 kJmol$^{-1}$ for CFO and 25.5 kJmol$^{-1}$ for CFO-LCO. The presence of adsorption in the OER is stated by the strongly negative value of $\Delta S^{\circ\#}$.

**Methanol Oxidation Reaction (MOR)**

**Cyclic Voltammetry (CV)**

The electrocatalysts were examined with regard to MOR by capturing Cyclic Voltammetry (CV) in 1M KOH and 1M $CH_3OH$ at 25°C as depicted in Fig. 6(A). CFO and CFO-LCO film electrodes exhibited high current density in 1M KOH and 1M $CH_3OH$ than that in 1M KOH. In the case of MOR,

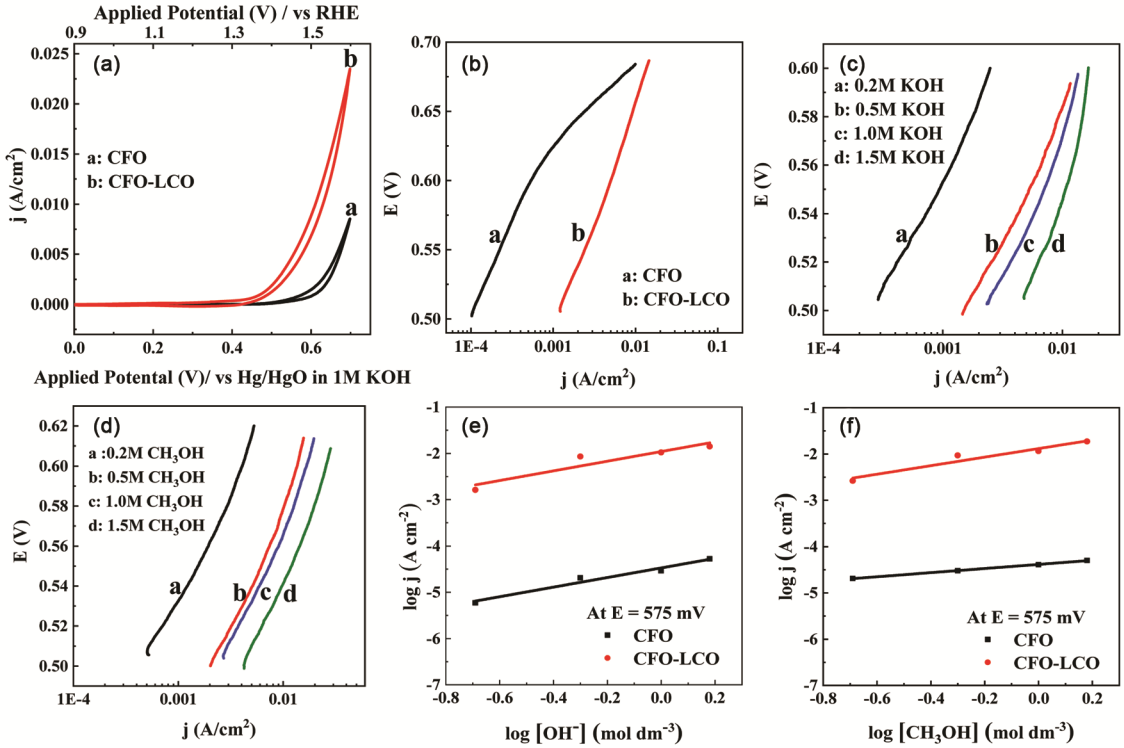


Fig. 6 — (A): CV Curve of Ni/CFO & CFO-LCO (scan rate = 20 mV/sec) in 1M KOH & 1M $CH_3OH$ at 25℃, (B):Anodic polarization curves for Ni/CFO & CFO-LCO in 1M KOH & 1M $CH_3OH$ at 25℃; scan rate: 0.2 $mVsec^{-1}$,(C): Anodic polarization curves for Ni/CFO-LCO at varying KOH concentrations at 25℃, (D): Anodic polarization curves for Ni/CFO-LCO at varying $CH_3OH$ concentrations at 25℃, (E): Plot of log j *vs* log [$OH^-$] for Ni/CFO & CFO-LCO electrodes at 575 mV, (F): Plot of log j *vs* log [$CH_3OH$] for Ni/CFO & CFO-LCO electrodes at 575 mV

Table 5 — Electrode kinetic parameters for CFO & CFO-LCO electrodesin 1M KOH & 1M $CH_3OH$ at 25° C

| Electrode | Loading (mg $cm^{-2}$) | Order | | Tafel Slope (b) | Apparent Current Density ($mA/cm^2$) at E = 650 mV | Specific activity ($mAcm^{-2}/g)\times10^{-3}$ at E = 650 mV |
|---|---|---|---|---|---|---|
| | | $p_{OH}$ | $p_{Me}$ | | | |
| CFO | 6.5 | 1.0 | 0.5 | 138 | 2.4 | 0.4 |
| CFO-LCO | 9.7 | 1.0 | 0.9 | 150 | 9.2 | 0.9 |
| 1M KOH & 1M $CH_3OH$ | | | | | | |

the current density enhances significantly in comparison with the OER, while the Ni(III)/Ni(II) redox peaks vanishes as reported in literature[74,75]. This is due to the strong interaction between the higher valence Ni(III) species and methanol and causes their nearly complete reduction under anodic conditions. Therefore, only a small amount of Ni(III) species remains for electrochemical reduction under cathodic conditions.

The onset potential for MOR has been compared for the electrocatalysts CFO & CFO-LCO and was found to be 0.58 V and 0.51 V, respectively. This clearly shows that the methanol oxidation starts at comparatively low potential with CFO-LCO film electrode.

## Electrocatalytic Activity

To determine the catalytic performance of the synthesized electrocatalysts with regard to MOR in alkaline medium, anodic polarization curve was recorded in 1M KOH and 1M $CH_3OH$ at 25°C as displayed in Fig. 6(B). The electrode kinetic parameters for MOR were estimated using the Tafel plot and values are presented in Table 5. When catalytic performance was compared in terms of current density at E = 650 mV, CFO-LCO (j = 9.2 $mAcm^{-2}$) film electrode was found to be more active towards MOR. This is due to change in morphology as supported by the SEM images.

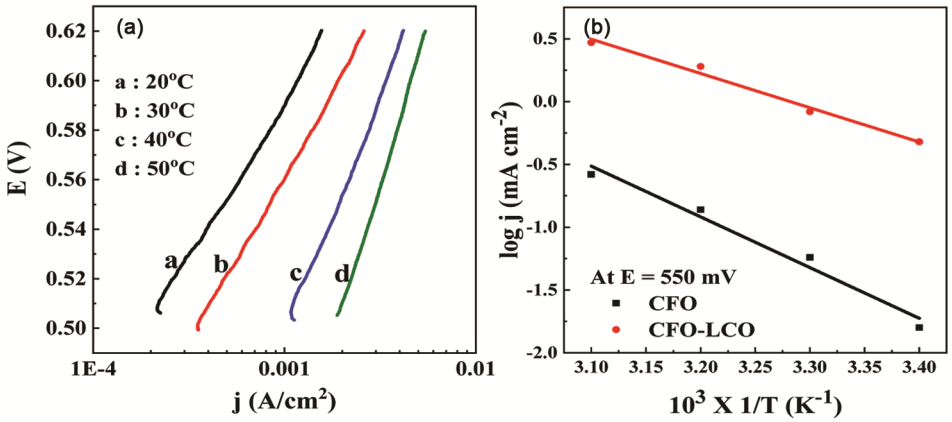


Fig. 7 — (A): Anodic Polarization Curve for Ni/CFO-LCO film electrode at different temperatures, (B): The Arrhenius plot for Ni/CFO &CFO-LCO at E = 550 mV in 1M KOH and 1M $CH_3OH$

Table 6 — Thermodynamic parameters for Ni/CFO & CFO-LCO in

| Electrode | $\Delta H_{el}^{\circ\#}$ (kJ $mol^{-1}$) at E = 550 mV | $\Delta S^{\circ\#}$ ($Jdeg^{-1}$ $mol^{-1}$) | $\Delta H^{\circ\#}$ (kJ $mol^{-1}$) |
|---|---|---|---|
| CFO | 77.4 | 115.7 | 101.1 |
| CFO- LCO | 52.3 | 174.1 | 66.3 |

The order of methanol oxidation reaction was evaluated by capturing the Tafel plots in various hydroxyl ion & methanol concentration (0.2M to 1.5M) at 25°C. The electrolytic solution's ionic strength was retained at 2.0 by employing $KNO_3$. A characteristic curve for CFO-LCO film electrode is presented in Fig. 6 (C)&(D). A log j *vs* log [$OH^-$] and log j *vs* log [$CH_3OH$] plot [Fig. 6(E)&(F)] was constructed for electrocatalysts at E = 575 mV. The order of reaction with respect to [$OH^-$] and [$CH_3OH$] was calculated by the gradient of straight line and values are tabulated in Table 5. The activity of the electrocatalysts is represented in the form of specific activity and is estimated by the equation (2) as discussed above.

## Thermodynamic Parameters

The thermodynamic study of MOR has been meticulously determined by the Tafel experiments conducted over a temperature window ranging from 20°C-50°C of 1M KOH and 1M $CH_3OH$. Fig. 7(A) depicts a characteristic curve obtained for CFO-LCO. The value of $\Delta H_{el}^{\circ\#}$ was determined from the gradient of log j *vs* 1/T plot [Fig. 7(B)].

Equation (3) and (4) were used to calculate $\Delta H^{\circ\#}$ and $\Delta S^{\circ\#}$ as discussed in the above section. The thermodynamic parameters were calculated for electrocatalysts and are given in the Table 6. The value of $\Delta H_{el}^{\circ\#}$ was found to be 77.4 $kJmol^{-1}$ for CFO and 52.3 $kJmol^{-1}$ for CFO-LCO.

## Conclusions

In order to investigate the effect of doping the lanthanum-based perovskite ($LaCoO_3$) in the cobalt-based spinel oxides ($CoFe_2O_4$) on the oxygen evolution and methanol oxidation reactions, $CoFe_2O_4$ (CFO)and $CoFe_2O_4$-$LaCoO_3$ (CFO-LCO) was synthesized by combining chemical co-precipitation and sol-gel techniques. The formation was physicochemically confirmed by FTIR and XRD. Composite material shows three-dimensional flower like morphology as confirmed from SEM images. CFO-LCO with its alluring form and unmatched electrocatalytic capabilities, represents a promising milestone on our journey towards advanced catalytic materials, poised to impact sustainable energy conversion processes with current densities of j = 1.6 $mAcm^{-2}$ and 9.2 $mAcm^{-2}$ at E = 650 mV for OER and MOR respectively.

## Acknowledgements

The Department of Chemistry, University of Lucknow, Lucknow is highly acknowledged for providing the necessary infrastructure to carry out the research work. Authors are thankful to the Higher Education Department, Govt. of Uttar Pradesh for financial support through Centre of Excellence

(COE). The Department of Science and Technology (DST), New Delhi is also thanked for providing an electrochemical workstation.

## References


1 Kim M, Lee C, Ko S M & Nam J-M N, *J Solid State Chem*, 270 (2019) 295.
2 Askari M B, Salarizadeh P, Seifi M & Rozati S M, *J Phys Chem Solids*, 135 (2019) 109103.
3 Abebe E M & Ujihara M, *ACS Omega*, 6 (2021) 23750.
4 Tahir M, Pan L, Idrees F, Zhang X, Wang L, Zou J-J & Wang Z L, *Nano Energy*, 37 (2017) 136.
5 Tahir M, Mahmood N, Pan L, Huang Z-F, Lv Z, Zhang J, Butt F K, Shen G, Zhang X & Dou S X, *J Mater Chem A*, 4 (2016) 12940.
6 Li Y, Hasin P & Wu Y, *Adv Mater*, 22 (2010) 1926.
7 Zhao Y, Jia X, Chen G, Shang L, Waterhouse G I, Wu L-Z, Tung C-H, O'Hare D & Zhang T, *J Am Chem Soc*, 138 (2016) 6517.
8 Chen R, Wang H-Y, Miao J, Yang H & Liu B, *Nano Energy*, 11 (2015) 333.
9 Wang Y, Zhou T, Jiang K, Da P, Peng Z, Tang J, Kong B, Cai W B, Yang Z & Zheng G, *Adv Energy Mater*, 4 (2014) 1400696.
10 Meng Y, Song W, Huang H, Ren Z, Chen S-Y & Suib S L, *J Am Chem Soc*, 136 (2014) 11452.
11 Bergmann A, Zaharieva I, Dau H & Strasser P, *Energy Env Sci*, 6 (2013) 2745.
12 Fekete M, Hocking R K, Chang S L, Italiano C, Patti A F, Arena F & Spiccia L, *Energy Environ Sci*, 6 (2013) 2222.
13 Najafpour M M, Ehrenberg T, Wiechen M & Kurz P, *Ang Chem Int Ed*, 49 (2010) 2233.
14 Smith R D, Prévot M S, Fagan R D, Zhang Z, Sedach P A, Siu M K J, Trudel S & Berlinguette C P, *Science*, 340 (2013) 60.
15 Feng J X, Ye S H, Xu H, Tong Y X & Li G R, *Adv Mat*, 28 (2016) 4698.
16 Zhu Y, Zhou W, Sunarso J, Zhong Y & Shao Z, *Adv Fun Mat*, 26 (2016) 5862.
17 Zhao X, Yin M, Ma L, Liang L, Liu C, Liao J, Lu T & Xing W, *Energy Environ Sci*, 4 (2011) 2736.
18 Qian L, Gu L, Yang L, Yuan H & Xiao D, *Nanoscale*, 5 (2013) 7388.
19 Ko T-H, Devarayan K, Seo M-K, Kim H-Y & Kim B-S, *Sci Rep*, 6 (2016) 1.
20 Parsons R & Vander N T, *J Electroanal Chem Interfacial Electrochem*, 257 (1988) 9.
21 Yu E H, Scott K & Reeve R W, *J Electroanal Chem.* , 547 (2003) 17.
22 Seland F, Harrington D A & Tunold R, *Electrochim Acta*, 52 (2006) 773.
23 Wasmus S & Küver A, *J Electroanal Chem*, 461 (1999) 14.
24 Kua J & Goddard W A J J o t A C S, *J Am Chem Soc*, 121 (1999) 10928.
25 Tanaka S, Umeda M, Ojima H, Usui Y, Kimura O & Uchida, *J Power Sources*, 152 (2005) 34.
26 Jiang J & Kucernak A, *J Electroanal Chem*, 543 (2003) 187.
27 Goodenough J, Hamnett A, Kennedy B, Manoharan R & Weeks S, *J Elect Chem Interfacial Electrochem*, 240 (1988) 133.
28 Sugimoto W, Saida T & Takasu Y, *Electrochem Communication*, 8 (2006) 411.
29 Park K-W, Ahn K-S, Nah Y-C, Choi J-H & Sung Y-E, *J Phys Chem B*, 107 (2003) 4352.
30 Biswas P, Nodasaka Y & Enyo M, *J Appl Electrochem*, 26 (1996) 30.
31 Prabhuram J, Zhao T, Liang Z & Chen R, *Electrochim Acta*, 52 (2007) 2649.
32 Zhao G-Y, Xu C-L, Guo D-J, Li H & Li H-L, *J Power Sources*, 162 (2006) 492.
33 Ohmori T, Nodasaka Y & Enyo M, *J Electroanal Chem Interfacial Electrochem*, 281 (1990) 331.
34 Machida K I & Enyo M, *Bull Chem Soc Jpn*, 58 (1985) 2043.
35 Machida K I & Enyo M, *J Electrochem Soc*, 137 (1990) 871.
36 Yadav S, Rani N & Saini K, Presented atIOP Conf Ser Mater Sci Eng, 2022.
37 Widiarti N, Sae J & Wahyuni S, Presented atIOP Conf Ser Mater Sci Eng, 2017.
38 Mehto A, Mehto V R, Chauhan J, Singh I & Pandey R, *J Nanomed Res*, 5 (2017) 00104.
39 Zhang Y, Sun X, Pan L, Li H, Sun Z, Sun C & Tay B K, *Solid State Ion*, 180 (2009) 1525.
40 Ghoreishi F, Ahmadi V & Samadpour M, *J Nanostruct*, 3 (2013) 453.
41 Durmus Z, Kurt B Z & Durmus A, *Chem Sel*, 4 (2019) 271.
42 Trinh L T, Quynh L A B & Hieu N H, *Int J Nanotechnol*, 15 (2018) 108.
43 Taufik A, Albert A & Saleh R, *J Photochem Photobiol A Chem*, 344 (2017) 149.
44 Gao Y, Wang L, Zhou A, Li Z, Chen J, Bala H, Hu Q & Cao X, *Mater Lett*, 150 (2015) 62.
45 Ye J S, Cui H F, Liu X, Lim T M, Zhang W D & Sheu F S, *Small*, 1 (2005) 560.
46 Mazabuel-Collazos A, Gómez C D & Rodríguez-Páez J, *Mater Chem Phys*, 222 (2019) 230.
47 Karthik K, Dhanuskodi S, Gobinath C & Sivaramakrishnan S,*Spectrochim Acta Part A Mol Biomol Spectrosc*, 139 (2015) 7.
48 Elemike E E, Onwudiwe D C & Singh M, *J Inorg Organomet Poly Mat*, 30 (2020) 400.
49 Bangruwa J S, Vashisth B K, Singh N, Singh N & Verma V, *J Alloys Compd*, 739 (2018) 319.
50 Liu X-M, Fu S-Y & Huang C-J, *Mater Sci Eng B*, 121 (2005) 255.
51 Muthu K S, Lakshminarasimhan N & Perumal P, *Solid State Sci*, 72 (2017) 33.
52 Singh H & Yadav K, *J Alloys Compd*, 585 (2014) 805.
53 Mo H-L, Jiang D-M, Wang C-M, Zhang W-G & Jiang J-S, *J Alloys Compd*, 579 (2013) 187.
54 Singh R N, Tiwari S K, Singh S P, Singh N K, Poillerat G & Chartier P, *J Chem Soc Faraday Trans*, 92 (1996) 2593.
55 Yakubu A, Abbas Z, Ibrahim N A & Hashim M, *Phys Sci Int J*, 8 (2015) 1.
56 Yoon S J, Lee S H, Kim K H & Ahn K S, *Mater Chem Phys*, 73 (2002) 330.
57 Habibi M H & Mardani M, *J Mol Liq*, 238 (2017) 397.
58 Saberi A, Golestani-Fard F, Sarpoolaky H, Willert-Porada M, Gerdes T & Simon R, *J Alloys Compd*, 462 (2008) 142.
59 Fradette N & Marsan B, *J Electrochem Soc*, 145 (1998) 2320.

60 Chaddha A S, Singh N K, Malviya M & Sharma A, *Sustain Energ Fuels*, 6 (2022) 2553.
61 Singh N K, Tiwari S K, Anitha K L & Singh R N, *J Chem Soc Faraday Trans*, 92 (1996) 2397.
62 Tiwari S K, Chartier P & Singh R N, *J Electrochem Soc*, 142 (1995) 148.
63 Adhikari S, Kwon Y & Kim D-H, *Chem Eng J*, 402 (2020) 126192.
64 Yadav R, Jhasaketan & Singh N K, *Int J Electrochem Sci*, 10 (2015) 9297.
65 Yadav R & Singh N K, *Ind J Chem*, 54A (2015) 1221.
66 Singh N K, Yadav R & Yadav M K, *J New Mater Electrochem Syst*, 19 (2016) 209.
67 Singh N K, Yadav R, Yadav M K & Fernandez C, *J New Mater Electrochem Syst*, 20 (2017) 115.
68 Yadav R & Singh N K, *Ind J Chem Tech*, 25 (2018) 189.
69 Wu W, Guo S & Zhang J, *Int J Electrochem Sci*, 13 (2018) 225.
70 Massot L, Chamelot P, Cassayre L & Taxil P, *Electrochim Acta*, 54 (2009) 6361.
71 Singh N K, Sharma P, Kumar I & Chaddha A S, *Int J Electrochem Sci*, 14 (2019) 11379.
72 Gileadi E, VCH Publishers Inc, New York, USA 1993.
73 Singh R N, Pandey J P, Singh N K, Lal B, Chartier P & Koenig J-F, *Electrochim Acta*, 45 (2000) 1911.
74 Singh R N, Singh A, Mishra D & Chartier P, *J Power Sources*, 185 (2008) 776.
75 Jadhav H S, Roy A, Chung W-J & Seo J G, *New J Chemistry*, 41 (2017) 15058.